



A new approach for modelling the fibre path in bolted joints of continuous fibre reinforced composites

Sven Roth*, Florian Pracisnore, Sven Coutandin, Jürgen Fleischer

wbk Institute of Production Science, Karlsruhe Institute of Technology (KIT), Karlsruhe, Germany

ARTICLE INFO

Keywords:

Bolted joints
Fibre conform hole forming
Fibre pathway
Analytical modelling
Continuous fibres

ABSTRACT

A fibre conform hole forming into continuous fibre reinforced components leads to beneficial part properties, as the fibre structure is not damaged in comparison to a drilling operation due to a reorientation of the fibres during the preforming process. To determine precisely the local component properties of the manufactured composite part, detailed information about the resulting fibre paths is required. For the first time, this paper provides a universal methodology to approximate the actual fibre paths in the reoriented area around the hole. Based on a few experimental data, the developed framework allows the construction of the fibre pathways depending on the formed hole diameter and the used fabric type. Two models based on polynomial splines are developed and compared with regards to the achievable model accuracy. The overall methodology is evaluated using different hole diameter and fabric types. Here, a very good correlation between approximation and reality is observed.

1. Introduction

Fibre reinforced plastics are characterized by their specific strength and stiffness values [1] and thus are often used in applications with high lightweight demands, for example in automotive or aviation [2]. Components with high mechanical requirements are mainly designed as continuous fibre reinforced structures, showing an uninterrupted fibre flow over the entire size of the composite part [3].

The joining of continuous fibre reinforced components is often realized by the use of bolted joints [4,5] or via embedded force transmitting elements [6,7]. Both methods require a hole in the composite part, which can either be drilled or realized during its manufacturing process through reorientation of the endless fibres [8]. Depending on the used materials and sample geometry, such a fibre conform hole forming leads to an increase in strength between 2.7% and 77% compared to drilled specimen [8–14].

To load-optimize the fibre course in fibre conform holes, different approaches have already been introduced. [15,16] considered for the first time the influence of a curvilinear fibre format on the reinforcing capacity of the fibre structure in circular holes and proposed to align the curved fibre path in the main stress direction. [17] transferred this approach into a finite element model, discretising the image of the continuously curved fibres in the hole area by using 18 linear fibre sections. [18] present a similar approach using a finite element model. Here, the discretization into linear fibre sections is realized by a parallel

running evolutionary algorithm, aiming to reduce stress peaks.

[19] and [20] also use a finite element approach to optimize the fibre course, whereas a distinction between near and far hole areas is done. The considered quadrant is discretized in $N \times M$ four-sided elements and a generic continuous material orthotropy distribution function (x) is constructed. In near hole areas, this function corresponds $N \times M$ piecewise to bilinear interpolations, which are each assigned to a $N \times M$ four-sided element. The proposed fibre course results from the material orthotropy design, chosen under the constraint to minimize the Tsai-Wu failure criterion and therefore maximizing the mechanical reinforcement.

An analytical approach to optimize the fibre course is presented in [21] and [22]. From a defined starting point, the fibre paths are mapped piecewise as a linear function. Their angle β_i to the starting point is equated to the angle between the components main stress direction and the stress distribution prevailing at the starting point.

Another approach for a fibre alignment along the main stress axis is presented by [23]. Here, a finite element model is used to determine the stress distribution, whereas small discrepancies between the main stress axis and the fibre orientation are permitted in areas of lower stress density. This approach is intended to counteract continuity disturbances and irregularities in the fibre arrangement.

All presented approaches focus on a stress-ideal fibre orientation in the hole area. However, the fibre orientation that is actually generated during the hole forming process is not considered. Merely [24] and

* Corresponding author.

E-mail addresses: sven.roth@kit.edu (S. Roth), sven.Coutandin@kit.edu (S. Coutandin), juergen.Fleischer@kit.edu (J. Fleischer).

[25,26] describe the resulting fibre orientation in the hole area in initial approaches, but are limited to hot hole forming of fibre reinforced thermoplastics: [24] derives the geometrical course of the maximum deflected fibre on the edge of the formed hole and, this way, describes the expansion behaviour during forming process. Furthermore, [25,26] present an approach to approximate the resulting fibre orientation of local heated reinforced thermoplastics using a cubic function. For its determination, two supporting points are estimated from CT images. By using only a qualitative comparison with CT images, the model accuracy remains unspecific. In addition, process influencing variables such as the hole diameter or different fabrics are not taken into account.

As shown, the existing approaches are not suitable to describe the actual fibre pathways after the fibre conform hole forming process or are limited in terms of transferability and accuracy. However, the knowledge of the fibre orientation generated during the hole forming is essential to determine precisely the local component properties [27,28]. Thus, the aim of this paper is to derive a universal methodology, allowing an exact description of the fibre courses for different hole diameters and fabrics. The presented approach considers existing process influencing variables and allows to redefine necessary model parameters based on a few experimental measurement series.

2. Materials and methods

2.1. Materials

Two different fibre fabrics were used for experimental data collection. On the one hand, a $-45^\circ/+45^\circ$ fabric with a grammage of 204 g/m^2 of the type HiMax™ FCIM253 produced by Hexcel Corporation was used [29]. On the other hand, a $0^\circ/90^\circ$ fabric with a grammage of 209 g/m^2 of the type CBXS200 produced by Lange + Ritter GmbH was employed [30]. Both textiles show the same fibre tex of 800 but differentiate in the stitching fibre.

2.2. Hole forming procedure

As a first step, one fabric layer with the size of $75 \times 75 \text{ mm}^2$ (Fig. 1, left picture) was inserted and fixed into the clamping frame, shown in Fig. 1 (centre picture). The subsequent hole forming was carried out by penetrating the textile using the piercing pins illustrated in Fig. 1 (right). To do so, a borehole with a diameter of 51 mm was placed in the lower part of the clamping frame. The point angle of both pins is 20° while having a diameter of 9.0 mm and 18.0 mm. For an orthogonal and centred piercing, a guiding tube was provided in the upper part of the clamping frame. The fixation of the resulting fibre orientation for further analysis was carried out by applying and activating the binder type EPIKOTE™ Resin 05,390 of Hexion Inc. using infrared heaters [31].

2.3. Fibre path characterization

The characterization of the fibre paths was carried out by evaluating macroscopic images with a resolution of 100 pixels/mm. With the help

of the image editing software GIMP V. 2.8.22, individual fibre courses were tracked manually at a distance of 1–2 mm along the y-axis, see Fig. 2 (left). In an interval of 1 mm along the x-axis, data points relative to the hole centre were collected, see Fig. 2 (right). The number of the resulting lines was selected in such a way that all fibres influenced by the hole formation were captured. The width of the area was set to 40 mm, as outside this region no significant influence of hole formation on the fibre orientation was observed in any of the samples. A total of 31.164 data points were collected for the following model testing. Table 1 provides an overview of the corresponding samples.

3. Methodology for the fibre path approximation

In this chapter, a universal methodology to approximate actual fibre pathways after a fibre conform hole forming in continuous fibre fabrics is presented. The aim of the resulting model is the analytical description of the curvilinear fibre paths depending on the material architecture and the diameter of the pin.

Initially it is necessary to specify the design of the functional model in order to allow a pertinent application on real samples. All developed models refer to specific fibres via their transition points, which represent the border between the unaltered and the deformed fibre area. Outside the deformed area, the trajectory of originally horizontal fibres is considered. Whereas the fibre paths inside the deformed area are described with the presented model. In order to facilitate the model construction, the origin of the Cartesian coordinate system is placed at the centre of the formed hole.

The model construction requires an incremental approach. First, typified curves representing the idealized fibre paths are designed. Therefore, the experimentally characterized fibre courses of several specimen are aggregated to average fibre paths for each parameter specification. Second, different polynomial splines are applied on the resulting typified curves. An assessment of particularly pertinent interpolation points takes place in order to refine the approximation of the idealized behaviour. In the final step, the elaborated spline characteristics are expressed as depending variables of the underlying parameters.

3.1. Generation of typified curves based on characterized fibre paths

3.1.1. Aggregation of experimentally characterized fibre courses

The purpose of typified curves is the representation of the fibre behaviour, abstracting stochastic distortions related to the experimental fibre path characterization. These distortions materialize in curve deflections without systematic patterns. Assuming a random distribution of the samples' distortions, it is reasonable to assume that they balance each other out when aggregating sufficient amounts of samples. This is the fundamental idea of the typified curves construction.

In this paper, two biaxial fabrics with an equal fibre distribution in both directions have been used. Therefore, symmetrical fibre courses with respect to both co-ordinate axis can be assumed. To obtain the required typified curves, an aggregation regarding the four quadrants of

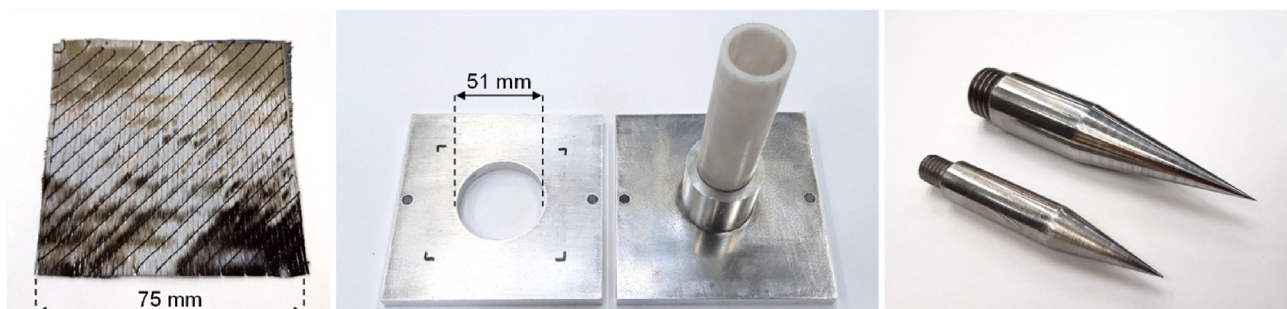


Fig. 1. Hole forming set-up: fibre fabric type HiMax™ FCIM253 (left), clamping frame (centre), piercing pins (right).

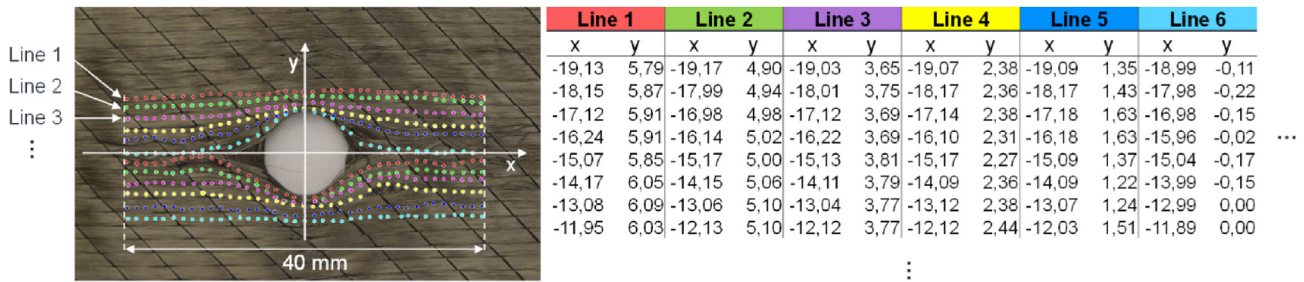


Fig. 2. Procedure for the fibre path characterization: tracking of the fibre courses (left), resulting data base (right).

Table 1
Number of samples.

	Pin diameter D	
	9 mm	18 mm
HiMax™ FCIM253 (-45°/+45°)	16 specimen	14 specimen
CBXS200 (0°/90°)	14 specimen	16 specimen

each specimen takes place in a first step, see Fig. 3. In a second step, all specimen with common parameter specifications contribute to an average set of curves. These typified curves represent the idealized fibre behaviour for each parameter set in table 1.

3.1.2. Standardized procedure for the determination of typified curves

To enable an automated and reproducible determination of the typified curves, a standardized aggregation method is established. It allows the identical processing of all experimental data points. The method requires a replicable definition of observation areas, including all transition points belonging to paths running above and below the hole. These two observation areas must be symmetrical regarding the abscissa axis. It has to be considered that they may overlap to a certain extent, as paths running above the hole can have their origin below the

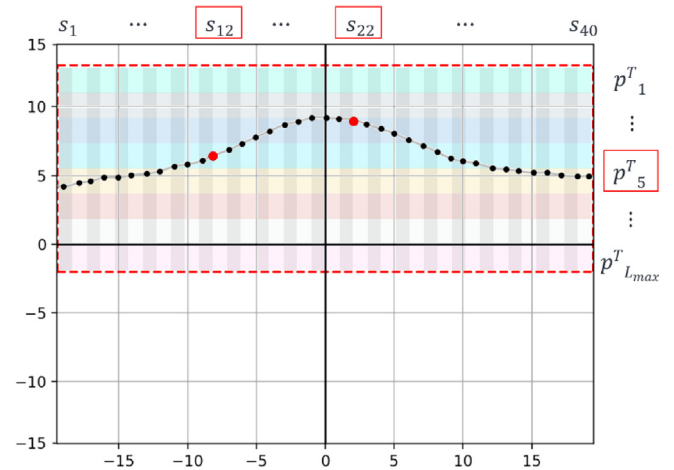


Fig. 4. Schematic assignment of two data points of path p_s^T for the upper observation area (axis value in mm).

hole centre and vice versa. Moreover, both observation areas must be centred with respect to the ordinate axis in order to meet the symmetry requirement.

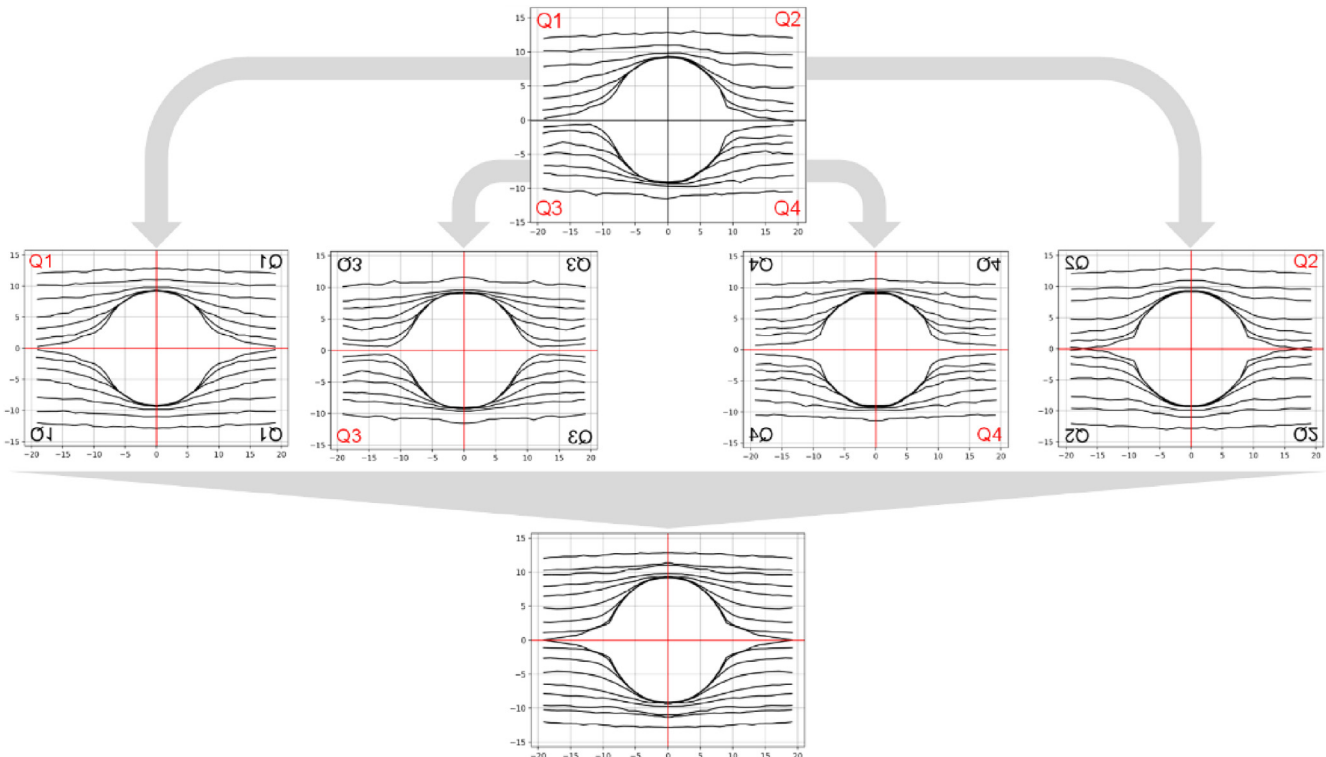


Fig. 3. Scheme of the aggregation on sample level.

In a first step, the two observation areas above and below the hole are partitioned vertically in L_{max} segments having the same width. L_{max} corresponds to the maximum number of paths observed above or below the hole. The segments of the upper observation area are numbered from bottom to top from 1 to L_{max} , indicated by different colours in Fig. 4. The segments of the lower observation area are numbered from 1 to L_{max} inversely from top to bottom. Then, the corresponding segment affiliation of a particular path point is determined by choosing the transition point with the lowest vertical distance to the considered segment.

In a second step a horizontal segmentation takes place. In the present study, a path typically consists of 39 points, having 19 or 20 points located on each side of the ordinate axis. Therefore, the observation area to the left and to the right of the ordinate axis is partitioned in 20 equidistant segments, preventing a systematic double segment allocation. The segments are labelled from s_1 to s_{40} in Fig. 4. For each path point, the segment allocation takes place depending on its horizontal distance as mentioned above. An exemplary allocation for two path points of pathway p_5^T is shown in Fig. 4. It should be noted, that symmetric segments with respect to the ordinate axis have a correspondence and therefore refer to the same aggregation area.

With the set framework, fibre path points of each quadrant are attributed to one of the $L_{max} \times 20$ aggregation areas. After the segment allocation, all points belonging to the same aggregation area are synthesized to one typified node. To do so, the mean values of the abscissa and ordinates of the corresponding points are computed. The resulting typified curves represent the fibre behaviour of one particular quadrant. The curves of the remaining quadrants are then mapped via axis mirroring.

3.2. Approximation of typified curves using splines

3.2.1. Chosen spline morphology

In this paper, the curves representing the actual behaviour are designed by using splines, as the degree of polynomials involved in the curve construction remains small. This is not the case when employing methods of interpolation or classical approximation due to the trade-off between degree of polynomials and error size.

Different spline morphologies appear to have substantially different suitability for the present use case: Bezier splines as well as B-splines are not interpolating. Akima- and Renner-sub-splines can be subjected to flexural fractures. Polynomial compensation splines require arbitrary weighting. Hermite-splines are characterized by high polynomial degree. Splines from these categories do not meet the construction criteria.

In contrast to this, basic cubic and quadratic splines show a low polynomial degree and a high aptitude for the present use case: By merging cubic splines, the resulting construction curve runs through the desired interpolation points and can be continuously differentiated twice over the entire definition range. Moreover, a construction condition enabling the specification of the value of a particular derivative in the two border points of the definition area can be employed to increase the accuracy of the curve. By replacing the cubic splines with quadratic splines at the two border areas, the respective number of degrees of freedom can be increased by one. This enables the specification of a further design condition related to a specific derivative in both ending points. Those two alternatives, which only differ in the degree of the polynomials at the borders, represent the construction scaffold of the two developed models. Here, model CS refers to plain cubic splines, whereas model MS refers to mixed cubic and quadratic splines.

When employing cubic and quadratic splines, symmetry requirements cannot be implemented without further ado. To keep the model simple, only the fibre behaviour of one quadrant will be approximated by splines. The entire construction curve can be constructed via axis mirroring. Thus, the borders of the definition range correspond to the

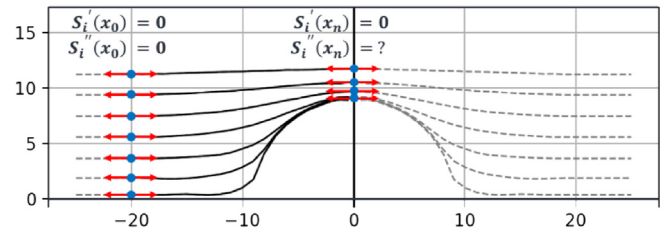


Fig. 5. Applicable conditions for the spline construction (axis value in mm).

transition area separating constant and deformed fibres and to the turning point above or below the hole. As illustrated in Fig. 5, the first and second derivative in the transition point can be set to zero to fulfil the requirement of smooth transitions. The point above or below the hole centre represents a global maximum. Therefore, the first derivative can be set to zero as well. A condition for the second derivative for the global maximum (or minimum) cannot be formulated just like that.

3.2.2. Selection of suitable interpolation points

To fulfil the demand of a high approximation accuracy, appropriate interpolation points have to be identified. Interpolation points refer to specific typified nodes of the typified curves, through which the splines will run. To define the error size of the approximated fibre pathways, the vertical distances between the spline curve and the nodes of the experimentally determined typified fibre paths can be summed up. Thus, the accuracy of the approximation can be evaluated depending on the position and number of interpolation points n . The range of possible interpolation point combinations corresponds to the number of different selections of n typified nodes out of the 20 nodes belonging to one quadrant. By defining start and end point, the number of possible combinations is slightly reduced. The start point of the spline construction corresponds to the transition point, the typified node of the first segment of each typified curve. The end point cannot be set to the typified node of the last segment, as a gap would most certainly appear when performing the axis mirroring. The end point must therefore lie on the ordinate axis, which will be referred to as point number 21*. As a consequence, $n - 2$ typified nodes out of the 19 must be specified.

Two different approaches appear for the selection of suitable interpolation points. The first one, here defined as run specific approach, has the advantage of simplifying further proceedings, see Fig. 6 (left). Here, all typified curves of the quadrant are considered simultaneously. A specific interpolation point of a particular interpolation point combination refers to all typified nodes belonging to the corresponding horizontal segment of each single typified curve. The second one, here defined as individual path approach, foresees an individual observation of each curve, see Fig. 6 (right). The selected interpolation point combination of the different typified curves can differ. Consequently, the approximation might be more accurate. It has to be assessed whether the benefits of increasing accuracy outweigh the disadvantages of more complex further proceedings.

3.3. Determination of model values

The nodes of each typified curve selected to be interpolation points have to be characterized. Here, the coordinates of an interpolation point are described depending on the material architecture and diameter of the pin. Furthermore, a dependency on the vertical position of the related typified curve is given. The value of the second derivative at turning point above or below the hole centre must be characterized depending on the same variables. Therefore, model values are categorized into two groups: purely parameter-dependent values and parameter and transition point -dependent values.

3.3.1. Purely parameter dependent variables

A variable v , having no dependency towards transition points, must

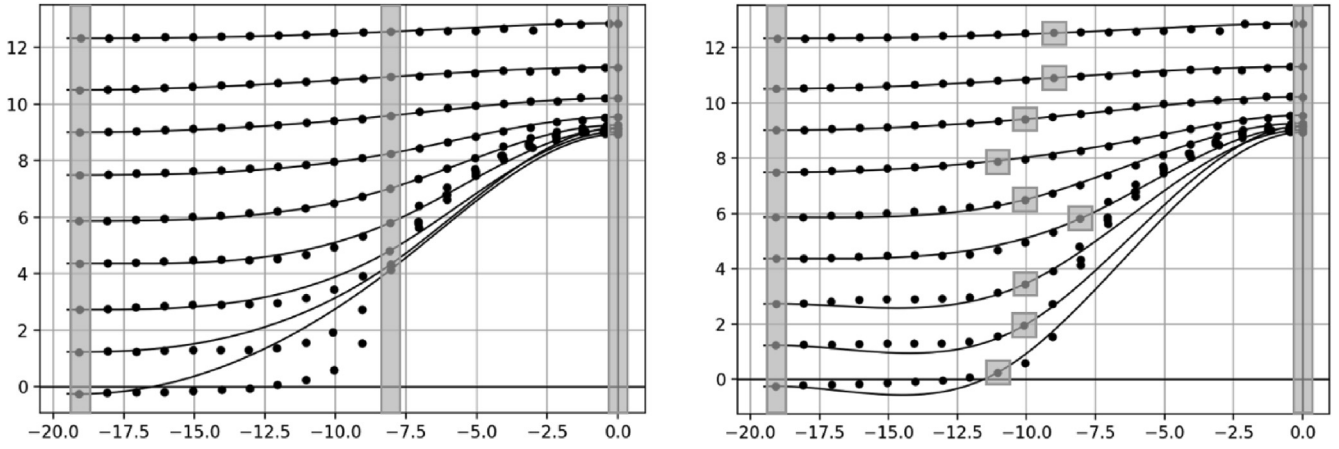


Fig. 6. Selection of suitable interpolation points: run specific approach (left); individual path approach (right) (axis value in mm).

be expressed depending on the two relevant parameters d , describing the diameter of the pin, and z , describing material architecture. In this paper, both parameters adopt two values. These sample specific circumstances enable a simple variable description based on linear systems and metrical translation of parameter characteristics. If further parameter values were available, the functional relationship between the value v and the parameters could easily be elaborated or a pertinent substitution function describing the dependency could be implemented.

Here, a metrical translation of the parameter characteristics is necessary. For the material architecture the $-45^\circ/45^\circ$ ply is arbitrarily set to 0 and $0^\circ/90^\circ$ ply is set to 1. For the diameter of the pin, the values 9 mm and 18 mm are adopted to keep the translation intuitive. For a variable v depending on the underlying parameter d and z with two respective values, formula 1 can be defined.

$$v(d, z) = \left(\frac{v_G - v_Y - \frac{v_B - v_R}{18 - 9}}{1 - 0} z + \frac{v_B - v_R}{18 - 9} \right) d + \left(\frac{(2v_Y - v_G) - (2v_R - v_B)}{1 - 0} z + (2v_R - v_B) \right), \quad (1)$$

$$v(18, 1) = v_G,$$

$$v(9, 1) = v_Y$$

$$v(18, 0) = v_B,$$

$$v(9, 0) = v_R.$$

3.3.2. Parameter and transition point dependent variables

In addition to the dependency towards the parameter d and z , some variables are dependent on the position of their related typified curve. The position can be characterized by the ordinates of the respective transition point. Thus, the considered variable adopts different values depending on the ordinate of the transition point.

The idea is to establish a functional relationship for every subsample group between the considered variable and the ordinate of the transition point. Ideally, this relationship has the same functional structure for all subsample groups. Here, the relationship's characteristics are expressed as functions of the parameters values as discussed above.

To approximate the relationship between the considered variable and the ordinates of the transition point, multiple analytical ways are conceivable. In total, L_{max} value pairs are considered for each single subsample group. In this paper, the discrete Gaussian least squares method is chosen. It has the disadvantage of requiring a functional system, which can be arbitrarily set. The methods advantage largely compensates its flaws: The resulting approximation expression can be

completed by further terms at any time, enabling continuous accuracy improvements, if required. For approximation purposes, algebraic polynomials, exponential terms and rational terms will be considered using the Gaussian least square method and compared in terms of resulting accuracy.

4. Experimental testing of the methodology and discussion:

Based on the materials and methods described in chapter 2, the introduced methodology for the fibre path approximation is tested experimentally. Therefore, an exemplary model expression is displayed and the resulting errors are evaluated.

4.1. Exemplary application of the method

4.1.1. Resulting typified curves and contribution score

Applying the approach presented in chapter 3.1, all characterized samples displayed in table 1 have been processed to their resulting typified curves, see Fig. 7. The aggregated curves show a smooth run around the hole and differ in their appearance depending on the pin diameter and material architecture.

To evaluate if the available data is sufficient for the curves to be representative for the fibre behaviour, the contribution of each specimen is computed. To do so, the impact of each data point of all specimens in one subsample group on the resulting construction curve is determined. Therefore, possible vertical displacements $V_{ij}(n)$ of the construction nodes (segment j , path i) along all typified curves are calculated. The distance is squared and aggregated to an impact score $V(n)$. To avoid distortions, only contributions to segments already occupied by a construction node are considered from the second specimen onwards. Thus, an accurate contribution assessment requires the measurement of the impact of specimens with high segment occupation rates at the beginning. Specimen with lower segment occupation rates are considered subsequently. This approach guarantees, that as few data points as possible remain unconsidered. Formula 2 and formula 3 describe the impact measurement for a given subsample group.

$$V_{ij}(n+1) = \left(\frac{\tilde{y}_{i,j}^{(n+1)} - [z_{i,j}(n+1) - z_{i,j}(n)] \tilde{y}_{i,j}^{(n)}}{z_{i,j}(n+1)} \right)^2 \cdot 1_{z_{i,j}(n) \neq 0} \quad (2)$$

$$V(n+1) = \sum_{i \in P^T} \sum_{j=0}^{40} V_{ij}(n+1) \quad (3)$$

$\tilde{y}_{i,j}^{(n)}$ – Ordinate of the data point of sorted specimen number n . In the case of multiple occupancy, the mean value of data points assigned to segment (i, j) is considered

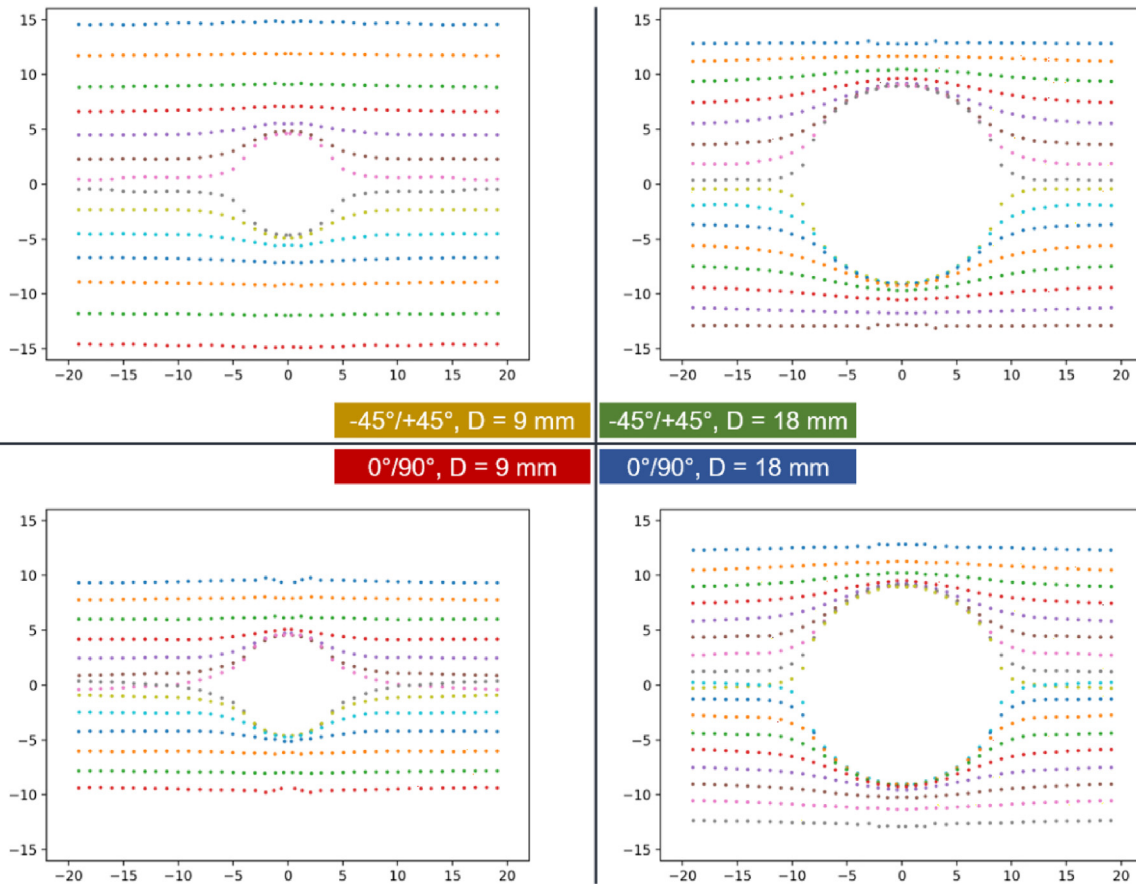


Fig. 7. Typified curves of the examined subsample groups (axis value in mm).

$y_{ij}^{-(n)}$ – Ordinate of the construction node of the first n sorted specimens

$z_{i,j}(n)$ – Number of (i, j) -segment occupations among the first n sorted specimens

P^T – Set of L_{max} typified curves

Table 2 displays the contribution of each individual specimen to the

construction curve. As shown, the impact of specimen no. 10 is below 0,00% in all four subsample groups. Further expanding the scope of considered specimen would hardly impact the resulting construction.

4.1.2. Evaluation of suitable interpolation points

Applying the approach presented in chapter 3.2, appropriate

Table 2

Impact of each individual specimen to the construction curve.

-45°/+45°, D = 9 mm Specimen no.	1	2	3	4	5	6	7	8	9	10
Amount of paths	7	6	5	5	5	5	5	5	5	5
Amount of segments	139	120	100	100	100	100	100	100	100	100
Accumulated contribution [mm ²]	10.472	10.500	10.507	10.507	10.508	10.509	10.509	10.509	10.509	10.510
Impact	100 %	0,26 %	0,06 %	0,01 %	0,01 %	0,00 %	0,00 %	0,00 %	0,00 %	0,00 %
-45°/+45°, D = 18 mm Specimen no.	1	2	3	4	5	6	7	8	9	10
Amount of paths	8	8	8	8	8	7	7	7	7	7
Amount of segments	160	160	160	158	158	140	140	140	140	140
Accumulated contribution [mm ²]	12.186	12.193	12.196	12.197	12.199	12.200	12.200	12.201	12.201	12.201
Impact	100 %	0,06 %	0,02 %	0,01 %	0,02 %	0,01 %	0,00 %	0,00 %	0,00 %	0,00 %
0°/90°, D = 9 mm Specimen no.	1	2	3	4	5	6	7	8	9	10
Amount of paths	7	7	7	7	6	6	6	6	6	6
Amount of segments	139	139	139	139	120	120	120	120	119	119
Accumulated contribution [mm ²]	4.280	4.318	4.322	4.323	4.323	4.323	4.324	4.324	4.324	4.324
Impact	100 %	0,88 %	0,10 %	0,02 %	0,01 %	0,01 %	0,01 %	0,01 %	0,01 %	0,00 %
0°/90°, D = 18 mm Specimen no.	1	2	3	4	5	6	7	8	9	10
Amount of paths	9	9	9	9	8	8	8	8	8	8
Amount of segments	180	178	178	177	160	160	160	160	160	160
Accumulated contribution [mm ²]	12.546	12.563	12.567	12.569	12.571	12.573	12.573	12.574	12.574	12.574
Impact	100 %	0,14 %	0,03 %	0,02 %	0,02 %	0,02 %	0,00 %	0,00 %	0,00 %	0,00 %

Table 3
Flaw size between the splines and the typified nodes for the parameter set 0°/90°, D = 18 mm (in mm²).

		IP 3		IP 4		IP 5		IP 6		IP 7	
		IP	Abs	IP	Abs	IP	Abs	IP	Abs	IP	Abs
Model CS											
Run specific	Total	[1, 8, 21*]	17,99	[1, 12, 13, 21*]	7,28	[1, 7, 10, 14, 21*]	1,76	[1, 8, 11, 13, 14, 21*]	0,74	[1, 5, 10, 11, 12, 14, 21*]	0,40
Path individual	L1	[1, 19, 21*]	0,04	[1, 13, 15, 21*]	0,02	[1, 12, 14, 15, 21*]	0,02	[1, 4, 8, 14, 15, 21*]	0,02	[1, 3, 4, 12, 14, 15, 21*]	0,02
	L2	[1, 20, 21*]	0,02	[1, 4, 19, 21*]	0,01	[1, 3, 15, 19, 21*]	0,01	[1, 3, 14, 17, 18, 21*]	0,01	[1, 3, 14, 17, 18, 19, 21*]	0,00
	L3	[1, 9, 21*]	0,02	[1, 4, 8, 21*]	0,01	[1, 7, 10, 13, 21*]	0,01	[1, 7, 12, 14, 16, 21*]	0,01	[1, 7, 12, 15, 16, 20, 21*]	0,01
	L4	[1, 14, 21*]	0,02	[1, 2, 13, 21*]	0,01	[1, 3, 11, 20, 21*]	0,00	[1, 2, 8, 10, 20, 21*]	0,00	[1, 2, 4, 8, 10, 20, 21*]	0,00
	L5	[1, 12, 21*]	0,04	[1, 7, 10, 21*]	0,01	[1, 6, 11, 18, 21*]	0,00	[1, 7, 9, 14, 17, 21*]	0,00	[1, 7, 9, 14, 18, 19, 21*]	0,00
	L6	[1, 9, 21*]	0,36	[1, 12, 17, 21*]	0,09	[1, 4, 11, 17, 21*]	0,01	[1, 6, 8, 11, 17, 21*]	0,00	[1, 6, 8, 12, 14, 17, 21*]	0,00
	L7	[1, 8, 21*]	1,59	[1, 12, 16, 21*]	0,40	[1, 5, 12, 13, 21*]	0,03	[1, 5, 12, 13, 20, 21*]	0,02	[1, 4, 9, 11, 13, 20, 21*]	0,01
	L8	[1, 7, 21*]	4,29	[1, 12, 14, 21*]	0,99	[1, 8, 11, 12, 21*]	0,13	[1, 9, 11, 12, 16, 21*]	0,04	[1, 5, 10, 11, 12, 16, 21*]	0,00
	L9	[1, 7, 21*]	8,79	[1, 9, 15, 21*]	3,79	[1, 8, 9, 14, 21*]	1,05	[1, 10, 11, 12, 13, 21*]	0,22	[1, 5, 10, 11, 12, 13, 21*]	0,08
	Total		15,18		5,32		1,26		0,32		0,13
Model MS											
Run specific	Total		(9, 15)*	4,33	(7, 10, 14)*	2,59	(9, 10, 13, 16)*	0,70	(10, 11, 12, 13, 17)*		0,44
Path individual	L1		(2, 20)	0,04	(12, 15, 19)	0,02	(6, 13, 15, 19)	0,02	(13, 15, 16, 17, 18)		0,01
	L2		(3, 19)	0,01	(3, 10, 11)	0,01	(3, 15, 17, 18)	0,00	(3, 7, 14, 17, 18)		0,00
	L3		(2, 17)	0,03	(3, 12, 20)	0,02	(4, 11, 16, 18)	0,01	(4, 12, 15, 16, 20)		0,01
	L4		(15, 20)	0,04	(3, 10, 20)	0,00	(2, 11, 15, 20)	0,00	(2, 9, 12, 15, 20)		0,00
	L5		(5, 10)	0,01	(3, 12, 18)	0,00	(5, 10, 14, 17)	0,00	(5, 11, 14, 15, 16)		0,00
	L6		(3, 12)	0,02	(5, 9, 13)	0,00	(5, 8, 11, 14)	0,00	(5, 8, 12, 14, 17)		0,00
	L7		(5, 11)	0,11	(5, 10, 12)	0,06	(5, 12, 13, 16)	0,02	(3, 9, 11, 13, 16)		0,01
	L8		(12, 13)	0,46	(9, 11, 12)	0,04	(9, 11, 12, 17)	0,02	(5, 10, 11, 12, 16)		0,00
	L9		(6, 10)	1,90	(8, 9, 14)	1,77	(9, 10, 13, 16)	0,29	(10, 11, 12, 13, 20)		0,07
	Total			2,62		1,93		0,38			0,10

interpolation points (IPs) have been identified for the two models CS and MS. Table 3 exemplary displays the accuracy of the approximation for the parameter set 0°/90° & D = 18 mm depending on the position and number of interpolation points *n*. The flaw size is expressed by the minimum aggregated distance between the splines and the typified nodes. Here, L1, L2, ..., L9 refer to the sum of the quadratic vertical distances between the nodes of a specific typified path and the corresponding spline path. Total represents the sum of the quadratic distances of all paths. As reasonably expected, an accuracy improvement with increasing number of considered interpolation points can be observed. Moreover, the individual path approach outperforms the run specific approach. However, the performance advantages vanish with increasing number of interpolation points considered.

4.1.3. Determination of model construction values

Depending on the accuracy requirements, the number of interpolation points is being set as shown above. The respective coordinates can then be expressed according to the relevant parameters and the corresponding typified curve via its transition ordinate *t*, see chapter 3.3.

When applying the run specific approach, the abscissa of the interpolation points is independent on the considered path. Thus, the abscissa can be expressed using formula 1. Yet, the ordinates, which dependent on the considered path, cannot be computed the same way. A function computing the value of the interpolation point ordinate depending on the transition ordinate *t* must be developed. Fig. 8 displays the relationship between the transition ordinate *t* and the ordinate *y* for an example with four interpolation points per quadrant. The relationship of the first interpolation point is always linear, as it refers to the transition point. Yet, all other relationships must be approximated.

In order to construct a numerical function depending on *t* for each single interpolation point ordinate, the Gaussian least square method was employed. Table 4 exemplary displays the approximation accuracy for the considered case of four interpolation points, using different functional systems for the parameter set 0°/90° & D = 18 mm. Accuracy is expressed as the mean squared distance between the actual and approximated value. Depending on the accuracy requirements, a selection of a pertinent approximation takes place. The corresponding

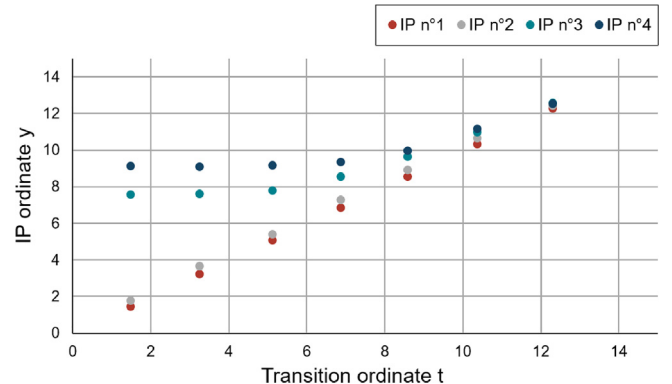


Fig. 8. Correlation between the transition ordinate *t* and the ordinate *y* for four interpolation points per quadrant (axis value in mm).

coefficients *k_i* can also be expressed using formula 1. The same approach is used to express the approximation of the second derivative.

4.2. Exemplary model expression

As an example for the analytical description of the fibre pathway, the CS model using four interpolation points per quadrant and the run specific approach is shown below, see formula 4, ..., formula 10 [32]. The variable *q* indicates whether the fibres are described above (*q* = 1) or below (*q* = -1) the hole. The expression can be derived by using basic cubic spline expressions considering four interpolation points. Here, the description area considers the ordinates of all transition points belonging to the pathways of a specific subsample group. The subsample specific *t_{min}* and *t_{max}* can be computed by considering the rectangle including all corresponding transition points belonging to the same subsample, see Fig. 9.

Here, the definition area corresponds to:

q = 1:

f: ℝ × [*t_{min}*, ∞) → ℝ,

Table 4
Approximation accuracy using different functional systems for the parameter set 0°/90°, D = 18 mm (in mm²).

	IP n°1		IP n°2		IP n°3		IP n°4	
	CS	MS	CS	MS	CS	MS	CS	MS
Polynomial functional system								
$y(t) = k_0 + k_1 \cdot t$	0,0	0,0	0,2471	0,0045	0,3982	0,4668	0,4108	0,4108
$y(t) = k_0 + k_1 \cdot t + k_2 \cdot t^2$	-	-	0,0292	0,0036	0,0201	0,0129	0,0395	0,0395
$y(t) = k_0 + k_1 \cdot t + k_2 \cdot t^2 + k_3 \cdot t^3$	-	-	0,0019	0,0016	0,0052	0,0123	0,0045	0,0045
$y(t) = k_0 + k_1 \cdot t + k_2 \cdot t^2 + k_3 \cdot t^3 + k_4 \cdot t^4$	-	-	0,0014	0,0014	0,0031	0,0007	0,0025	0,0025
$y(t) = k_0 + k_1 \cdot t + k_2 \cdot t^2 + k_3 \cdot t^3 + k_4 \cdot t^4 + k_5 \cdot t^5$	-	-	0,0014	0,0013	0,0015	0,0004	0,0024	0,0024
Exponential functional system								
$y(t) = k_0 + k_1 \cdot e^t$	-	-	4,0818	9,3758	2,4540	0,9891	0,3050	0,3050
$y(t) = k_0 + k_1 \cdot e^t + k_2 \cdot e^{2t}$	-	-	1,9500	5,5568	0,9966	0,2744	0,0432	0,0432
$y(t) = k_0 + k_1 \cdot e^t + k_2 \cdot e^{2t} + k_3 \cdot e^{3t}$	-	-	0,8911	3,2550	0,3492	0,0503	0,0083	0,0083
$y(t) = k_0 + k_1 \cdot e^t + k_2 \cdot e^{2t} + k_3 \cdot e^{3t} + k_4 \cdot e^{4t}$	-	-	0,3426	1,7377	0,0995	0,0075	0,0042	0,0042
$y(t) = k_0 + k_1 \cdot e^t + k_2 \cdot e^{2t} + k_3 \cdot e^{3t} + k_4 \cdot e^{4t} + k_5 \cdot e^{5t}$	-	-	0,0666	0,7034	0,0084	0,0015	0,0031	0,0031
Rational functional system								
$y(t) = k_0 + k_1/t$	-	-	7,5252	13,0184	5,2997	2,8726	1,5172	1,5172
$y(t) = k_0 + k_1/t + k_2/t^2$	-	-	3,3304	4,1546	2,8240	1,8721	1,1335	1,1335
$y(t) = k_0 + k_1/t + k_2/t^2 + k_3/t^3$	-	-	0,7738	0,8026	0,7886	0,7416	0,5870	0,5870
$y(t) = k_0 + k_1/t + k_2/t^2 + k_3/t^3 + k_4/t^4$	-	-	0,1012	0,0797	0,1069	0,1413	0,2084	0,2084
$y(t) = k_0 + k_1/t + k_2/t^2 + k_3/t^3 + k_4/t^4 + k_5/t^5$	-	-	0,0097	0,0088	0,0089	0,0084	0,0311	0,0311

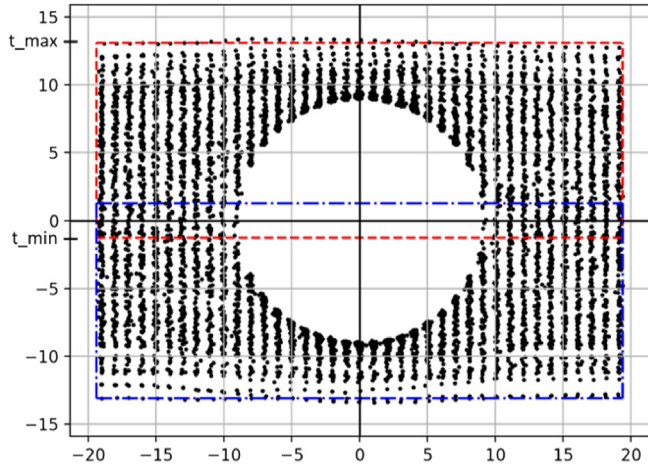


Fig. 9. Description area for the parameter set 0°/90°, D = 18 mm (axis value in mm).

$q = -1$:

$$f: \mathbb{R} \times (-\infty, -t_{min}] \rightarrow \mathbb{R}$$

The subsample specific values for t_{min} and t_{max} can be expressed as functions of the parameters using again formula 1. The function expression is composed as follows:

$$\text{For } t \notin [\min[q \cdot t_{max}, t_{min}], \max[q \cdot t_{min}, t_{max}]]: f(x, t) = t. \quad (4)$$

$$\text{For } t \in [\min[q \cdot t_{max}, t_{min}], \max[q \cdot t_{min}, t_{max}]]$$

$$f(x, t) = \begin{cases} a(x, t) + b(x, t) \cdot (x - v(x)) + c(x, t) \cdot (x - v(x))^2 + d(x, t) \cdot (x - v(x))^3, & x \in [x_0, x_6], \\ t, & t, x \notin [x_0, x_6]. \end{cases} \quad (5)$$

The coefficient a (constant term) is defined as:

$$a(x, t) = \begin{cases} a_0(t \cdot q) \cdot q, & \& x \in [x_0, x_1] \cup [x_5, x_6] \\ a_1(t \cdot q) \cdot q, & \& x \in [x_1, x_2] \cup [x_4, x_5], \\ a_2(t \cdot q) \cdot q, & \& x \in [x_2, x_4] \end{cases}, \text{ with } \begin{cases} a_0(t) = t, \\ a_1(t) = y_1(t) \\ a_2(t) = y_2(t). \end{cases} \quad (6)$$

Coefficient b (first degree term) is defined as:

$$b(x, t) = \begin{cases} b_0(t \cdot q) \cdot q, & x \in [x_0, x_1] \\ b_1(t \cdot q) \cdot q, & x \in [x_1, x_2] \\ b_2(t \cdot q) \cdot q, & x \in [x_2, x_3] \\ -b_2(t \cdot q) \cdot q, & x \in [x_3, x_4] \\ -b_1(t \cdot q) \cdot q, & x \in [x_4, x_5] \\ -b_0(t \cdot q) \cdot q, & x \in [x_5, x_6] \end{cases}, \text{ with:}$$

$$b_0(t) = \frac{s_0(t)}{h_0} - \frac{h_0}{3} \cdot [c_1(t) + 2c_0(t)],$$

$$b_1(t) = \frac{s_1(t)}{h_1} - \frac{h_1}{3} \cdot [c_2(t) + 2c_1(t)],$$

$$b_2(t) = \frac{s_2(t)}{h_2} - \frac{h_2}{3} \cdot [l(t) + 2c_2(t)],$$

$$l(t) = -\frac{1}{2 \cdot h_2} \cdot [3 \cdot s_2(t) + h_2 \cdot c_2]. \quad (7)$$

Coefficient c (second degree term) is defined as:

$$c(x, t) = \begin{cases} c_0(t \cdot q) \cdot q, & x \in [x_0, x_1] \cup [x_5, x_6] \\ c_1(t \cdot q) \cdot q, & x \in [x_1, x_2] \cup [x_4, x_5], \\ c_2(t \cdot q) \cdot q, & x \in [x_2, x_4] \end{cases}$$

$$c_0(t) = \frac{1}{2 \cdot h_0} \cdot \left[3 \cdot \frac{y_{IS_2}(t) - t}{h_0} - c_1(t) \cdot h_0 \right],$$

$$c_1(t) = \frac{\left(\frac{9}{2} \cdot \frac{s_2(t)}{h_2} - 3 \cdot \frac{s_1(t)}{h_1} \right) \cdot h_1 - \left(3 \cdot \frac{s_1(t)}{h_1} - \frac{9}{2} \cdot \frac{s_0(t)}{h_0} \right) \cdot \left(2 \cdot h_1 + \frac{3}{2} \cdot h_2 \right)}{h_1^2 + \left(\frac{3}{2} \cdot h_0 + 2 \cdot h_1 \right) \cdot \left(2 \cdot h_1 + \frac{3}{2} \cdot h_2 \right)},$$

$$c_2 = \frac{\left(3 \cdot \frac{s_1(t)}{h_1} - \frac{9}{2} \cdot \frac{s_0(t)}{h_0} \right) \cdot h_0 - \left(\frac{9}{2} \cdot \frac{s_2(t)}{h_2} - 3 \cdot \frac{s_1(t)}{h_1} \right) \cdot \left(2 \cdot h_1 + \frac{3}{2} \cdot h_0 \right)}{h_1^2 + \left(\frac{3}{2} \cdot h_0 + 2 \cdot h_1 \right) \cdot \left(2 \cdot h_1 + \frac{3}{2} \cdot h_2 \right)}. \quad (8)$$

Coefficient d (third degree term) is defined as:

$$d(x, t) = \begin{cases} d_0(t \cdot q) \cdot q, x \in [x_0, x_1] \\ d_1(t \cdot q) \cdot q, x \in [x_1, x_2] \\ d_2(t \cdot q) \cdot q, x \in [x_2, x_3] \\ -d_2(t \cdot q) \cdot q, x \in [x_3, x_4] \\ -d_1(t \cdot q) \cdot q, x \in [x_4, x_5] \\ -d_0(t \cdot q) \cdot q, x \in [x_5, x_6] \end{cases}, \text{ with:}$$

$$d_0(t) = \frac{1}{3 \cdot h_0} \cdot (c_1(t) - c_0(t)),$$

$$d_1(t) = \frac{1}{3 \cdot h_1} \cdot (c_2(t) - c_1(t)),$$

$$d_2(t) = \frac{1}{3 \cdot h_2} \left(-\frac{3}{2} \cdot \frac{s_2(t)}{h_2^2} - \frac{3}{2} \cdot c_2(t) \right),$$

$$v(x) = \begin{cases} x_0, x \in [x_0, x_1] \\ x_1, x \in [x_1, x_2] \\ x_2, x \in [x_2, x_3] \\ x_3, x \in [x_3, x_4] \\ x_4, x \in [x_4, x_5] \\ x_5, x \in [x_5, x_6] \end{cases}, \text{ and: } \begin{cases} h_i = x_{i+1} - x_i, \\ s_i(t) = y_{i+1}(t) - y_i(t) \\ \text{for } i \in \{0, 1, 2\} \end{cases} \quad (9)$$

The term $v(x)$ refers to the left border of the abscissa segment to which the abscissa x belongs. The expressions h_i and $s_i(t)$ serve to simplify the handling and calculation of the coefficients defined above. The arithmetic average of the abscissa of all collected data points belonging to the same segment is used to compute the corresponding abscissa value of the segment. The abscissa and ordinates of the relevant interpolation points x_i are constructed as described above.

The coordinates of the second interpolation point $IPn^{\circ}2$ are exemplary displayed in formula 10. For the ordinate expression an approximation based on a polynomial functional system meeting the accuracy requirements has been chosen.

$$x_{IPn^{\circ}2}(d, z_M) = (0, 2211 \cdot z_M - 0, 2227) \cdot d + (-2, 9893 \cdot z_M - 7, 0382),$$

$$y_{IPn^{\circ}2}(t) = (0, 076899 \cdot z_M - 0, 010456) \cdot d$$

$$+ (-1, 087494 \cdot z_M + 0, 602595), + (-0, 013949 \cdot z_M$$

$$+ 0, 023432) \cdot d + (0, 319355 \cdot z_M + 0, 584911) \cdot t$$

$$+ (0, 001037 \cdot z_M - 0, 002255) \cdot d$$

$$+ (-0, 026899 \cdot z_M + 0, 038585) \cdot t^2 \quad (10)$$

4.3. Evaluation of the model accuracy

To evaluate the model accuracy, the experimental characterized fibre pathways are compared to the exemplary expressed splines from chapter 4.2, using again four interpolation points each quadrant. The graphical assessment of the models indicates a good approximation of model CS and MS. Fig. 10 shows the modelled splines (white curves) compared to the characterized fibre pathways (coloured dots) of a random sample. The transitions in unaltered fibre areas are smooth and the underlying dynamics of the fibre pathways around the hole are recreated accurately. By comparing further samples it can be concluded, that the presented approach is suitable to qualitatively describe the actual fibre pathways after the hole forming process.

To further quantitatively evaluate the approximation results of model CS and MS, the overall average vertical distance of collected data points to their respective modelled pathways is computed. Table 5 shows the resulting error relative to the width of the fibre deformation area $[-t, t_{max}^f]$ for all specimen for each subsample group. The distance ratios suggest solid model quality, whereas both models show almost the same accuracy despite a negligible difference in for the parameter set $0^\circ/90^\circ$ & $D = 18$ mm. It should be noted, that the shown model error can be improved significantly by adding further interpolation points to the spline expression.

5. Conclusion

The presented methodology provides a framework, allowing the approximation of fibre pathways after the fibre conform hole forming process in fibre textiles. In contrast to previous investigations by [15-23] on a stress-ideal fibre orientation in the hole area, this approach allows the consideration of the fibre orientation that is actually generated during the hole forming. Thus, providing detailed information to determine precisely the local component properties. Compared to [24] and [25,26], the two presented model variants are capable to describe the fibre pathways universally for all types of endless fibre material. Since the methodology is based on a constructional approach, the model accuracy improves with the amount of available experimental data. In the present study, the data of only 3–4 specimen per subsample group turned out to be sufficient to achieve a good model quality, clearly exceeding current attempts.

The consideration of the constructional approach as well as the use case application of models CS and MS reveal the capabilities but also certain limits of the developed models itself. First of all, the optical evaluation of the resulting fibre pathways modelled by CS and MS is highly convincing: The dynamics of the displaced pathways are recreated accurately around the central hole. Moreover, the modelled transition between the deformed and unaltered fibre area is particularly accurate. The advantage of the chosen approach lies in the very nature of underlying instruments: Using splines guarantees computational simplicity due to the involved low-grade polynomials. Moreover, the approach enables accuracy refinement at any time using different adjusting levers discussed above. Eventually, the possibility of considering different conditions at the boundaries enables the modelling of different geometries, meaning that the application of the developed approach is not limited to the considered use-case.

Yet, the application of the models reveals certain flaws which have to be acknowledged. The developed methodology can only be applied to situations, where the data allows a reconstruction of the ideal fibre behaviour. If this is not the case, the model will lose its general descriptive character. Moreover, both models are yet designed employing the two existing parameter hole diameter and fabric type, enabling an exact description of parameter-dependent variables as linear systems. The presented approach allows an extension for further possible parameter values, but the underlying relations would have to be examined more closely and the extension would have to be suitably designed for a high model accuracy.

Finally, in some cases, the analytical description of the second derivative value leads to faulty fibre pathways when using the MS model. Here, the problem does not refer to the approximation, but rather to the determination of the empirical values on which the approximation is based on. One way to avoid this circumstance is to reduce the degree of freedom of the spline construction by one at the corresponding border. Thus, the mixed spline construction uses a quadratic function in the transition area and considers cubic polynomials elsewhere. However, it is assumed that the results of this hybrid construction would hardly differ from the results of the CS model.

CRediT authorship contribution statement

Sven Roth: Conceptualization, Methodology, Validation, Formal analysis, Writing - original draft, Visualization, Supervision, Project administration. **Florian Pracisnore:** Methodology, Software, Validation, Formal analysis, Writing - original draft, Visualization. **Sven Coutandin:** Writing - review & editing, Project administration. **Jürgen Fleischer:** Writing - review & editing, Project administration, Funding acquisition.

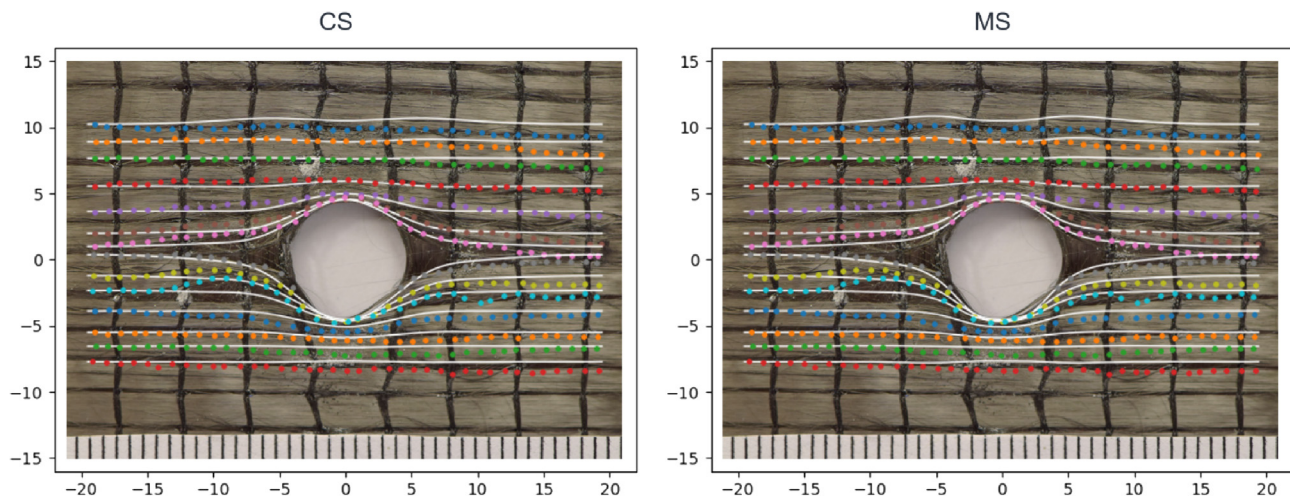


Fig. 10. Qualitative comparison of model CS and MS to a random sample of the parameter set $0^\circ/90^\circ$, $D = 18$ mm (axis value in mm).

Table 5

Relative error of collected data points to their respective modelled pathways.

	$0^\circ/90^\circ$, $D = 18$ mm	$0^\circ/90^\circ$, $D = 9$ mm	$-45^\circ/+45^\circ$, $D = 18$ mm	$-45^\circ/+45^\circ$, $D = 9$ mm
CS	0,37%	0,39%	0,35%	0,31%
MS	0,37%	0,38%	0,35%	0,31%

Declaration of Competing Interest

The authors declare that they have no known competing financial interests or personal relationships that could have appeared to influence the work reported in this paper.

Acknowledgements

This work was supported by the German Research Foundation (DFG: Deutsche Forschungsgemeinschaft, Project-No.: 418238897).

Data availability

The raw/processed data required to reproduce these findings cannot be shared at this time due to technical or time limitations.

Appendix A. Supplementary data

Supplementary data to this article can be found online at <https://doi.org/10.1016/j.compstruct.2020.112184>.

References

- Fleischer J, Teti R, Lanza G, Mativenga P, Möhring H-C, Caggiano A. Composite materials parts manufacturing. *CIRP Ann* 2018;67(2):603–26.
- Njuguna J. *Lightweight Composite Structures in Transport: Design, Manufacturing, Analysis and Performance*. s.l.: Elsevier Science; 2016.
- Henning F, Kärger L, Dörr D, Schirmaier FJ, Seuffert J, Bernath A. Fast processing and continuous simulation of automotive structural composite components. *Compos Sci Technol* 2019;171:261–79.
- Heimbs Sebastian, Schmeer Sebastian, Blaurock Jörg, Steeger Stefan. Static and dynamic failure behaviour of bolted joints in carbon fibre composites. *Compos A Appl Sci Manuf* 2013;47:91–101.
- Martinsen K, Hu SJ, Carlson BE. Joining of dissimilar materials. *CIRP Ann* 2015;64(2):679–99.
- Gebhardt J, Fleischer J. Experimental Investigation and Performance Enhancement of Inserts in Composite Parts. *Procedia CIRP* 2014;23:7–12.
- Ferret B, Anduze M, Nardari C. Metal inserts in structural composite materials manufactured by RTM. *Compos A Appl Sci Manuf* 1998;29(5):693–700.
- Chang L-W, Yau S-S, Chou T-W. Notched strength of woven fabric composites with moulded-in holes. *Composites* 1987;18(3):233–41.
- Durante M, Langella A. Bearing Behavior of Drilled and Molded-in Holes. *Appl Compos Mater* 2009;16(5):297–306.
- Lin HJ, Lee YJ. Strength of composite laminates with continuous fiber around a circular hole. *Compos Struct* 1992;21(3):155–62.
- Lin HJ, Tsai CC, Shie JS. Failure analysis of woven-fabric composites with moulded-in holes. *Compos Sci Technol* 1995;55(3):231–9.
- Nakai Asami, Ohki Takeru, Takeda Nobuo, Hamada Hiroyuki. Mechanical properties and micro-fracture behaviors of flat braided composites with a circular hole. *Compos Struct* 2001;52(3):315–22.
- Gebhardt J, Schwennen J, Lorenz F, Fleischer J. Structure optimisation of metallic load introduction elements embedded in CFRP. *Prod Eng Res Devel* 2018;12(2):131–40.
- Hufenbach W, Adam F, Helms O, Kupfer R. Gestaltung von textilverbundgerechten Fügezonen mit warmgeformten Bolzenlöchern. *Zeitschrift Kunststofftechnik / J Plast Technol* 2010;6:255–69.
- Hyer MW, Charette RF. Use of curvilinear fiber format in composite structure design. *AIAA J* 1991;29(6):1011–5.
- W. Hyer M, F. Charette R. Innovative design of composite structures: Use of curvilinear fiber format to improve structural efficiency 1987.
- Hyer MW, Lee HH. The use of curvilinear fiber format to improve buckling resistance of composite plates with central circular holes. *Compos Struct* 1991;18(3):239–61.
- Cho HK, Rowlands RE. Optimizing Fiber Direction in Perforated Orthotropic Media to Reduce Stress Concentration. *J Compos Mater* 2009;43(10):1177–98.
- Huang J, Haftka R, Rapoff A. Optimization Design of Composite Plates with Holes for Increased Strength. In: 44th AIAA/ASME/ASCE/AHS/ASC Structures, Structural Dynamics and Materials Conference. [Reston, Va.]: [American Institute of Aeronautics and Astronautics]; 2003, 335–341.
- Huang J, Haftka RT. Optimization of fiber orientations near a hole for increased load-carrying capacity of composite laminates. *Struct Multidisc Optim* 2005;30(5):335–41.
- Malakhov AV, Polilov AN. Design of composite structures reinforced curvilinear fibres using FEM. *Compos A Appl Sci Manuf* 2016;87:23–8.
- Malakhov AV, Polilov AN. Construction of trajectories of the fibers which bypass a hole and their comparison with the structure of wood in the vicinity of a knot. *J Mach Manuf Reliab* 2013;42(4):306–11.
- Zhu Yingdan, Liu Jiancai, Liu Dong, Haibing Xu, Yan Chun, Huang Bin, et al. Fiber path optimization based on a family of curves in composite laminate with a center hole. *Compos B Eng* 2017;111:91–102.
- Leiser J. Beitrag zu innovativen Verbindungstechniken für Hochleistungsverbundwerkstoffe. Zugl.: Chemnitz, Techn. Univ., Diss., 2006. Chemnitz: Inst. für Allg. Maschinenbau und Kunststofftechnik; 2006.
- Hufenbach W, G R, Kupfer R. Bolted joints with moulded holes for textile thermoplastic composites. *ICCM International Conferences on Composite Materials* 2011.
- Kupfer R. Zur Warmlochformung in Textil-Thermoplast-Strukturen Technologie, Phänomenologie, Modellierung [Dissertation]: Technische Universität Dresden; 2016.
- Malakhov AV, Polilov AN. Design algorithm of rational fiber trajectories in arbitrarily loaded composite plate. *J Mach Manuf Reliab* 2017;46(5):479–87.
- Malakhov AV, Polilov AN, Tian X. Progressive failure analysis of variable stiffness composite structures. In: AIP Conference Proceedings 2053, 030038; 2018; 1–4.
- Hexcel Corporation. Product Data Sheet: HiMax™ FCIM253 [C12k, 200, -45/+45]; 2016.
- Lange + Ritter GmbH. Product Data Sheet: CBXS200 Code Nr. 05300000209; n.d.
- Hexion Inc. Product Data Sheet: EPIKOTE™ Resin 05390; 2012.
- Engeln-Müllges G, Niederderren K, Wodicka R. *Numerik-Algorithmen: Verfahren, Beispiele, Anwendungen*. 10th ed. s.l.: Springer-Verlag; 2011.